JNS 2 (2012) 131-137

Journal of
NANOSTRUCTURES
JNS.kashanu.ac.ir

Preparation and Characterization of Downconversion Luminescent $LaVO_4$: Tm^{3+}, Yb^{3+} and Tm^{3+}/Yb^{3+} Nanosheets

M. Zahedifar[*a,b] , Z. Chamanzadeh[a]

[a]*Institute of Nanoscience and Nanotechnology, University of Kashan Kashan, I.R. Iran*

[b]*Faculty of Physics, University of Kashan, Kashan,I.R.Iran*

Article history:
Received 28/4/2012
Accepted 29/5/2012
Published online 1/6/2012

Keywords:
$LaVO_4$ Tm^{3+}/Yb^{3+}
Nanosheets
Downconversio
Nanostructures
Hydrothermal

**Corresponding author:*
E-mail address:
zhdfr@kashanu.ac.ir
Phone: 983615912838
Fax: +98 3615514005

Abstract

Tm^{3+}, Yb^{3+} and Tm^{3+}/Yb^{3+} doped $LaVO_4$ nanostructures were synthesized for the first time by using the hydrothermal method with the aid of $La(CH_3CO_2)_3$ as lanthanum source in presence of oleic acid as surfactant. The products were characterized by X-ray diffraction (XRD), scanning electron microscopy (SEM), transmission electron microscopy (TEM), photoluminescence (PL) spectroscopy and UV–Vis diffuse reflectance spectroscopy. Besides, the effects of activator concentration and sensitizer on the emission intensity were investigated. The PL spectrum revealed that the emission intensity decreases with increase in the concentration of Tm^{3+}, while adding Yb^{3+} as sensitizer causes the emission intensity to increase. The $LaVO_4$: Tm^{3+}/Yb^{3+} may possibly have potential application in enhancing the conversion efficiency of dye-sensitized solar cells by increasing the absorption of dyes.

1. Introduction

Nanomaterials are of current interest owing to their unique properties and potential applications in catalysis, optoelectronic devices, and so on [1-9]. Luminescent nanocrystals (NCs) that are soluble in organic solvents and polymers attract a great deal of interest since these materials can easily be processed via spin-coating techniques to form a uniform film from an organic solution [10]. Rare-earth (RE) doped luminescent materials have been the focus of many scientists due to their widely use in many different fields, such as phosphor [11, 12], biomedical applications [13] and laser host materials [14]. Also, the luminescent materials are very useful for spectrum modification through down shifting (DS), down conversion (DC) and up conversion (UC) in order to solar spectra modification for the efficiency en-

hancement of solar cells, because one major energy loss in solar cells is the thermalization of charge carriers generated by the absorption of high energy photons or the spectral mismatch between the incident solar photon spectrum and the band gap of semiconductor [15-19]. For example the irreversible electrochemical and thermal degradation of the dye or electrolyte components, originating from UV irradiation affects the chemical stability of Dye-Sensitized Solar Cells (DSSCs) and the common strategy to avoid the UV light is using a down conversion material to absorb UV rays and down convert it to visible light, which is reabsorbed by dye in DSSCs [20]. Lanthanide orthovanadates such as $LaVO_4$ are a significant rare earth luminescence family [21] due to their unique electronic structure and the numerous transition modes involving the 4f shell of rare earth ions [22]. Lanthanide orthovanadates generally crystallize in two polymorphs, monoclinic (m-) and tetragonal (t-). $LaVO_4$ has a monazite structure at ordinary pressures and a zircon structure at high pressures [23]. m-$LaVO_4$ is not a suitable host for luminescent activators [24] but t-$LaVO_4$ is expected to have superior properties. Sometimes, the efficiency that was observed or expected for photoluminescence emission in spectra conversion was low in singly doped media, because the direct excitation of the lanthanide ions is a relatively inefficient process, due to the forbidden character of the 4f transitions but it was quickly noticed that the mechanism could be made 1-2 orders of magnitude more efficient by use of ytterbium (Yb^{3+}) as a sensitizer ion in addition to the active ion, namely, erbium, holmium, or thulium. Energy transfer from a host material or other ion with a higher absorption coefficient could lead to much more efficient materials [25-27]. In this work, the synthesis of lanthanide-doped $LaVO_4$ nanocrystals by using the hydrothermal method is presented. Tm^{3+} was used as an activator ion in $LaVO_4$ nanocrystals to create emission spectra. For increase the efficiency of emission spectra, Yb^{3+} also was added as a sensitizer. These nanocrystals provide the possibility to excite most of the lanthanide ions via the charge-transfer transition within the vanadate group, followed by energy transfer to the emissive Tm^{3+}/Yb^{3+}. The characterization of the as-synthesized $LaVO_4$ nanocrystals was performed by using X-ray diffraction (XRD), scanning electron microscopy (SEM), transmission electron microscopy (TEM), UV–Vis diffuse reflectance spectroscopy analysis (UV–Vis) and photoluminescence (PL) spectroscopy.

2. Experimental

2.1. Synthesis

The $La_{(1-x)}VO_4$: Tm_x^{3+} (x= 0.005, 0.01, 0.02, 0.04) and $La_{0.98}VO_4$: $Yb_{0.02}^{3+}$ and $La_{0.8}VO_4$: $Tm_{0.01}^{3+}/Yb_{0.19}^{3+}$ nanocrystals were synthesized using a hydrothermal procedure. In a typical experimental procedure, 5 ml of oleic acid and 5 ml ethanol was added to a solution of 0.3 g NaOH and 0.03 g NH_4VO_3 dissolved in 2.5 ml DI water, while was stirring with vigorous magnetic stirrer. Then, a solution of $La(CH_3CO_2)_3.x\ H_2o$ and $Tm(NO_3).5H_2O$ (1 mmol total) was slowly added to the above solution at room temperature. After stirring for 30 min, the reactants were put into a 50 ml capacity teflon-lined autoclave. The autoclave was maintained at 140°C for 4 h and then cooled down to room temperature naturally. The NCs could be collected at the bottom of the vessels, and washed with cyclohexane and absolute ethanol for several times and dried in oven at 50°C for 10 h. Similarly, $LaVO_4$: Yb^{3+} were synthesized using $La(CH_3CO_2)_3.\ xH_2o$, $YbCl_3.H_2O$ with a molar ratio of 0.98: 0.02 and Also, $LaVO_4$: Tm^{3+}/Yb^{3+} were prepared by $La(CH_3CO_2)_3.\ xH_2o$, $YbCl_3.H_2O$ and $Tm(NO_3).5H_2O$ with a molar ratio of 0.8: 0.19: 0.01.

2.2. Characterization

X-ray diffraction (XRD) patterns were recorded by a Philips-X'pertpro, X-ray diffractometer using Ni-filtered CuK_{α} radiation at scan range of 2θ (0-70). A LEO 1455VP scanning electron microscope (SEM) was used to investigate the morphology of the product. Transmission electron microscope (TEM) images and high-resolution TEM (HRTEM) image were obtained on a JEM-2100 transmission electron microscope with an accelerating voltage of 200 kV. Room temperature photoluminescence (PL) properties of the product were studied on a Perkin-Elmer (LS 55) fluorescence spectrophotometer. The electronic spectra of the complexes were taken on a Shimadzu Ultraviolet–visible (UV–vis) scanning spectrometer (Model 2101 PC).

3. Results and discussion

X-ray powder diffraction (XRD) patterns of $LaVO_4$ nanocrystals at room temperature are shown in Fig. 1. Fig. 1a, 1b, 1c, and 1d as the patterns of $La_{(1-x)}VO_4$: Tm_x^{3+} (x= 0.01, 0.04), $La_{0.98}VO_4$: $Yb_{0.02}^{3+}$ and $La_{0.8}VO_4$: $Yb_{0.19}^{3+}/Tm_{0.01}^{3+}$ nanocrystals respectively. The result indicate that the as-prepared $La_{0.99}VO_4$: $Tm_{0.01}^{3+}$, $La_{0.98}VO_4$: $Yb_{0.02}^{3+}$ and $La_{0.8}VO_4$: $Tm_{0.01}^{3+}/Yb_{0.19}^{3+}$ NCs (Fig. 1a, 1c, 1d) are well crystallized and all of the peaks can be well fitted with the tetragonal (t-) phase of $LaVO_4$ with zircon structure (JCPDS Fill No. 32-0504) and the space group of *I41/amd* and lattice constants a = b = 7.49 Å and c = 6.59 Å. Additionally, no other peak can be found in the patterns, revealing that a pure phase t-$LaVO_4$ can be obtained. From XRD data, the crystallite diameter (D_c) of $La_{0.99}VO_4$: $Tm_{0.01}^{3+}$ nanocrystals were calculated to be 9-100 nm using the Scherer equation; $D_c = K\lambda/\beta\cos\theta$ [28] where β is the width of the observed diffraction line at its half intensity maximum (2 0 0), K is the so-called shape factor, which usually takes the value of about 0.9, and λ is the wavelength of X-ray source used in XRD. The XRD pattern of $La_{(1-x)}VO_4$: Tm_x^{3+} with different x (x = 0.005, 0.02) is similar to Fig. 1a, but increasing the amount of Tm^{3+} to x= 0.04 mmol leads to traces of tetragonal phase, which indicates that some of the Tm^{3+} ions crystallized as $TmVO_3$ and they cannot enter the lattice of $LaVO_4$, as shown in Fig. 1b which is in accordance with JCPDS (32-0504) and (25-0899).

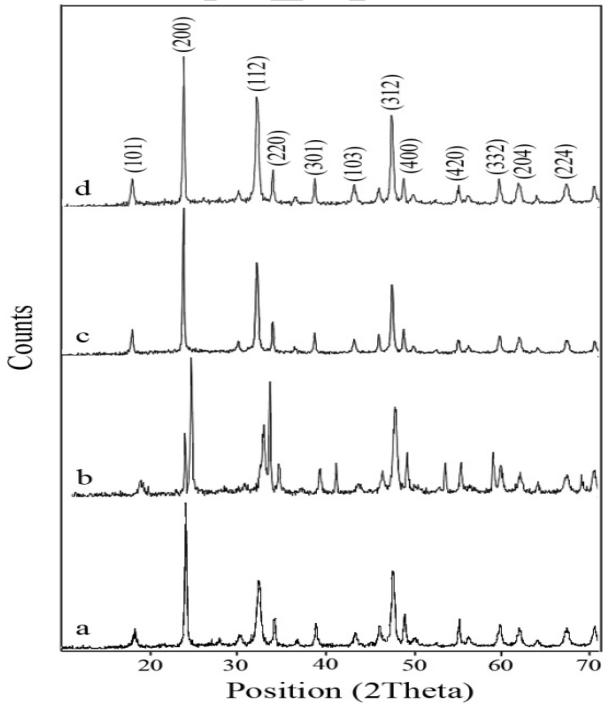

Fig. 1. XRD patterns of: (a) $La_{0.99}VO_4$: $Tm_{0.01}^{3+}$ (b) $La_{0.96}VO_4$: $Tm_{0.04}^{3+}$ (c) $La_{0.98}VO_4$: $Yb_{0.02}^{3+}$and (d) $La_{0.8}VO_4$: $Tm_{0.01}^{3+}/Yb_{0.19}^{3+}$ nanocrystal.

Also, the position of diffraction peaks move a slight towards the higher angles and the unit cell parameter is decreased since the ionic radius of Yb^{3+} is smaller than that of Tm^{3+}, therefore the crystallinity increased [29], when we change the activator ion from Tm to Yb element. The morphologies of $LaVO_4$: Tm^{3+} nanocrystals are investigated by scanning electron

microscopy (SEM). SEM images of $LaVO_4$: Tm^{3+} nanocrystals are shown in Fig. 2.

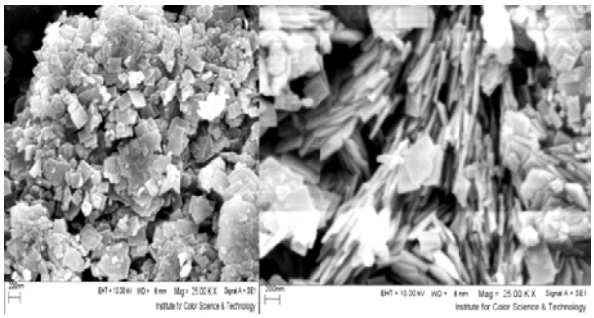

Fig. 2. SEM images of $LaVO_4$: Tm^{3+} nanocrystals

From the micrograph, it was observed that the as-prepared samples mainly composed of sheet-like morphology with an average length and diameter of 70 and 10 nm, respectively. These nanocrystals with irregular shapes were easily aggregated together. To further investigate the details of the morphology, TEM images were taken and shown in Fig. 3a, 3b and 3c. The size of nanosheets are about 50-150 nm, almost consistent with that observed from SEM image. The HRTEM image of the nanocrystals is shown in Fig. 3d, where the lattice fringe is measured to be 0.32 nm corresponding to the (2 0 0) lattice plane of tetragonal $LaVO_4$. It could be easily inferred from this image that these $LaVO_4$: Tm^{3+} nanosheets are single crystalline, uniform structure and free from defects in the examined area. Fig. 4 is the UV–Vis spectrum of the as-synthesized $La_{0.99}VO_4$: $Tm_{0.01}{}^{3+}$ nanosheets dispersed in cyclohexane.

The UV-Vis diffuse reflectance spectra of sample show an absorption band in UV region with a maximum at 280 nm. This absorption peak of $VO_4{}^{3-}$ groups is caused by a charge-transfer transition from the oxygen legends to the central vanadium atom in the V-O bond [10].

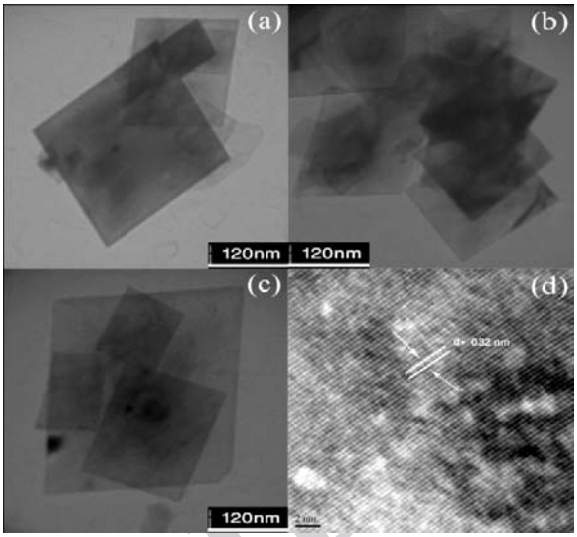

Fig. 3. TEM (a, b, c) and HRTEM (d) images of as-synthesized $LaVO_4$: Tm^{3+} nanosheets.

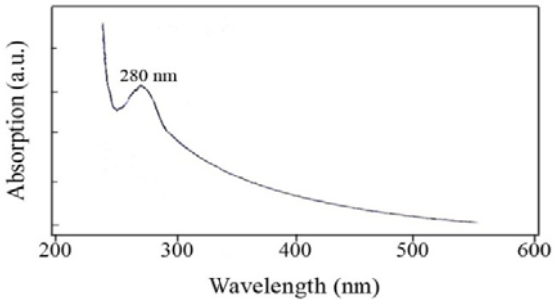

Fig. 4. UV-Vis diffuses reflectance spectra of $La_{0.99}VO_4$: $Tm_{0.01}{}^{3+}$ nanosheets.

Also, the UV-Vis spectra of $LaVO_4$: Yb^{3+} and $LaVO_4$: Tm^{3+}/Yb^{3+} NCs are similar to $La_{0.99}VO_4$: $Tm_{0.01}{}^{3+}$. Therefore, the absorption spectrum is not dependent on the type of activator or sensitizer ion and it is related to the host lattice of $LaVO_4$ NCs. The downconversion luminescence of $La_{(1-x)}VO_4$: $Tm_x{}^{3+}$ (x= 0.005, 0.01, 0.02, 0.04) and $La_{0.98}VO_4$: $Yb_{0.02}{}^{3+}$ and $La_{0.8}VO_4$: $Tm_{0.01}{}^{3+}/Yb_{0.19}{}^{3+}$ nanocrystals were investigated. The room temperature PL spectra of the $La_{(1-x)}VO_4$: $Tm_x{}^{3+}$ NCs recorded in cyclohexane are shown in Fig. 5. These $La_{(1-x)}VO_4$: $Tm_x{}^{3+}$ NCs can emit spectral peaks in region 400-500 nm. The downconversion emission bands centered at 437 nm

and 480 nm correspond to $^1D_2 \rightarrow {}^3F_4$ and $^1G_4 \rightarrow {}^3H_6$ transitions of Tm^{3+} ions, respectively. The PL intensity of $LaVO_4$: Tm^{3+} NCs as a function of the activator ion concentration are shown in Fig. 6. It can deduced that the relative emission of $La_{(1-x)}VO_4$: Tm_x^{3+} NCs with lower Tm concentrations (x= 0.01 and 0.005) is much more intense and almost constant, but the emission intensity of $La_{(1-x)}VO_4$: Tm_x^{3+} NCs is decreased with increasing Tm^{3+} concentration.

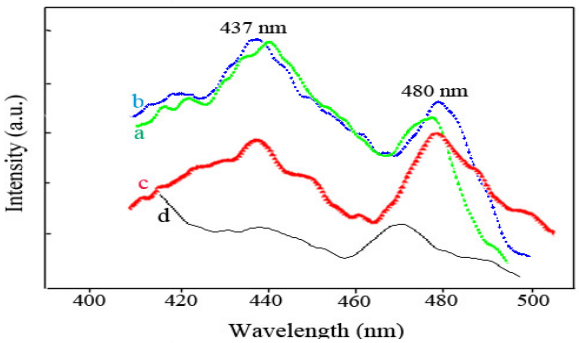

Fig. 5. The emission spectra of $La_{1-x}VO_4$:Tm_x^{3+}: (a) x = 0.005, (b) x = 0.01, (c) x = 0.02, (d) x = 0.04.

This behavior results from concentration quenching of Tm^{3+}. The excess of Tm^{3+} ions causes the self interaction between adjoining Tm^{3+} ions and results in lower transitions from $^1G_4$ and $^1D_2$ levels. Eventually, the emission intensities of $^1G_4 \rightarrow {}^3H_6$ and $^1D_2 \rightarrow {}^3F_4$ transitions are diminished [30]. The emission spectra of $La_{0.98}VO_4$: $Yb_{0.02}^{3+}$ nanocrystals are shown in Fig. 7.

This sample with Yb^{3+} as activator emits spectra peak in region 700-800 nm, which can be ascribed to the transition of Yb^{3+} energy level from $^2F_{5/2} \rightarrow {}^2F_{7/2}$. Yb^{3+} ion has a single excited state $^2F_{5/2}$ above the ground state $^2F_{7/2}$, so it can emit photons at near infrared (NIR). Generally, Yb^{3+} has been used as sensitizer ion and according to the literature 17-20% Yb^{3+} is optimal doping [31,32]. So we chose 19% doping of Yb^{3+} and 1% Tm^{3+} as optimum value of Tm^{3+} according to Fig. 6, co-doped in $La_{0.8}VO_4$: $Tm_{0.01}^{3+}/Yb_{0.19}^{3+}$ nanocrystals.

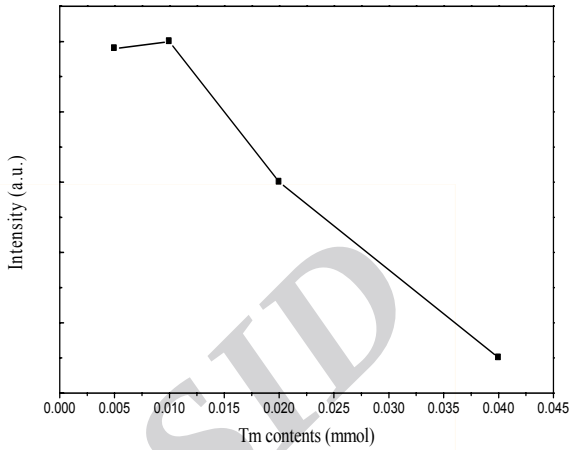

Fig. 6 The PL intensity of $LaVO_4$: Tm^{3+} NCs as a function of the activator ion concentration.

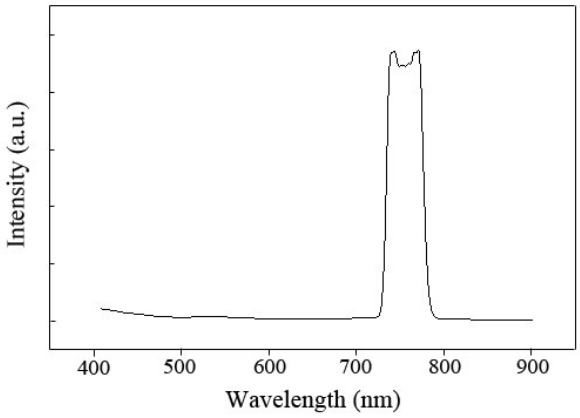

Fig. 7. The emission spectra of $La_{0.98}VO_4$: $Yb_{0.02}^{3+}$ nanocrystals.

Fig. 8 shows, the emission bands of $La_{0.8}VO_4$: $Tm_{0.01}^{3+}/Yb_{0.19}^{3+}$ nanocrystals centered at 434, 485, 510, 543 and 724 nm correspond to the $^1D_2 \rightarrow {}^3F_4$, $^1G_4 \rightarrow {}^3H_6$, $^1G_4 \rightarrow {}^3F_4$ and $^3F_3 \rightarrow {}^3H_6$ transitions of Tm^{3+} ions and NIR emission at 750 nm attributed to the $^2F_{5/2} \rightarrow {}^2F_{7/2}$ transition of Yb^{3+}. Therefore, Yb^{3+} ions act as a sensitizer and the efficient operative energy transfer take place from Yb^{3+} ions to their

neighbor Tm^{3+} ions and also cause the active excited state $^1G_4$ and $^3F_3$ of Tm^{3+}. As can be seen, more emission peaks are present in $La_{0.8}VO_4$: $Tm_{0.01}{}^{3+}/Yb_{0.19}{}^{3+}$ nanocrystals and the emission peak is intense comparing with $LaVO_4$: Tm^{3+} and $LaVO_4$: Yb^{3+}.

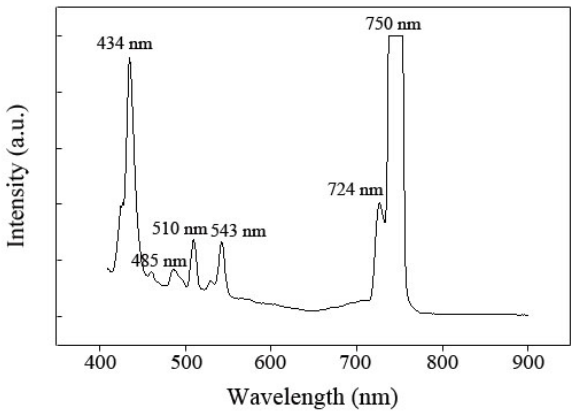

Fig. 8. The emission spectra of $La_{0.8}VO_4$: $Tm_{0.01}{}^{3+}/Yb_{0.19}{}^{3+}$ nanocrystals.

Fig. 9 shows the absorption spectra of a Ru phenanthroline complex (Ru(dcphen)$_2$) (NCS)$_2$), as photosensitizer in the dye-sensitized solar cells, with a broad absorption band in region 400-700 nm [33]. Therefore, it may have potential to reabsorb the emitted light by $LaVO_4$: Tm^{3+}/Yb^{3+} and regenerate excitons and enhance the photovoltaic conversion of dye solar cells.

In comparison with other methods, this process is simple, low cost, scale-up route and uses nontoxic precursor and solvent. Also for the first time, the hydrothermal method was used to synthesis of $LaVO_4$: Tm^{3+} NCs. In this route, Yb^{3+} was utilized as sensitizer for improvement of photoluminescence properties and the effect of activator materials on the photoluminescence characteristics was investigated.

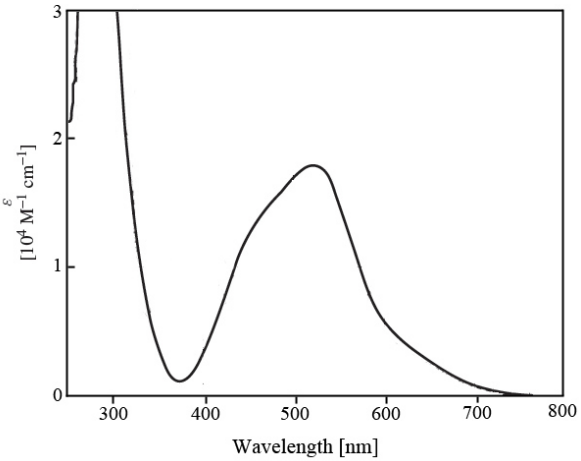

Fig. 9. The absorption spectra of a Ru phenanthroline complex (Ru (dcphen)$_2$) (NCS)$_2$) [34].

4. Conclusion

In summary, $LaVO_4$: Tm^{3+}, Yb^{3+} and Tm^{3+}/Yb^{3+} nanocrystals were successfully synthesized through a hydrothermal method. As-synthesized nanocrystals show $LaVO_4$: Tm^{3+}, Yb^{3+} and Tm^{3+}/Yb^{3+} phase with tetragonal structure without any other impurities. The luminescent properties of $LaVO_4$: Tm^{3+} has been improved with decreasing the molar concentration of Tm^{3+} ions. The PL measurements showed that $LaVO_4$: Tm^{3+}/Yb^{3+} nanocrystals could emit much more intense luminescence downconversion than $LaVO_4$: Tm^{3+} nanocrystals. Therefore, $LaVO_4$: Tm^{3+}/Yb^{3+} nanocrystals can be potentially used as downconversion material for enhancing the dye-sensitized solar cell efficiency.

Acknowledgment

Authors are grateful to research council of University of Kashan for providing financial support to undertake this work.

References

[1] T. Mishra, Catal. Commun. 9 (2008) 21.
[2] Z. Y. Zhou, N. Tian, J. T. Li, I. Broadwell, S. G. Sun, Chem. Soc. Rev. 40 (2011) 4167.

[3] M. Panzer, K. E. Aidala, V. Bulovic, nano. Rev. 3 (2012) 16144.
[4] B. Varghese, B. Mukherjee, K. R. G. Karthik, K. B. Jinesh, S. G. Mhaisalkar, E. S. Tok, C. H. Sow, J. Appl. Phys. 111 (2012) 104306.
[5] L. W. Chang, Y. C. Sung, J. W. Yeh, H. C. Shih, J. Appl. Phys. 109 (2011) 074318.
[6] H. Qu, L. Cao, G. Su, W. Liu, Y. Sun, B. Dong, J. Appl. Phys. 106 (2009) 093506.
[7] W. U. Huynh, J. J. Dittmer, A. P. Alivisatos, Science. 295 (2002) 2425.
[8] M. Haridas, J. K. Basu, D. J. Gosztola, G. P. Wiederrecht, Appl. Phys. Lett. 97 (2010) 083307.
[9] T. M. Jovin, Nat. B. 21 (2003) 32.
[10] J. Liu, Y. D. Li, Adv. Mater. 19 (2007) 1118.
[11] T. Higuchi, Y. Hotta, Y. Hikita, S. Maruyama, Y. Hayamizu, H. Akiyama, H. Wadati, D. G. Hawthorn, T. Z. Regier, R. I. R. Blyth, G. A. Sawatzky, H. Y. Hwang, Appl. Phys. Lett. 98 (2011) 071902.
[12] M. W. Blair, L. G. Jacobsohn, B. L. Bennett, R. E. Muenchausen, S. C. Sitarz, J. F. Smith, D. W. Cooke, P. A. Crozier, R. Wang, Mater. Res. Soc. Symp. Proc. 1056 (2007) HH07.
[13] M. Wang, G. Abbineni, A. Clevenger, C. Mao, S. Xu, Nanomedicine. 7 (2011) 710.
[14] A. B. Seddon, Z. Tang, D. Furniss, S. Sujecki, T. M. Benson, Opt. Express. 18 (2010) 26704.
[15] C. Strumpel, M. Mccann, G. Beaucarne, V. Arkhipov, A. Slaoui, V. Svrcek, C. Delcanizo, I. Tobias, Sol. Energ. Mat. Sol. Cel. 91 (2007) 238.
[16] E. Klampaftis, D. Ross, K. R. Mcintosh, B. S. Richards, Sol. Energ. Mat. Sol. Cel. 93 (2009) 1182.
[17] B. S. Richards, Sol. Energ. Mat. Sol. Cel. 90 (2006) 2329.
[18] M. Liu , Y . Lu , Z. B. Xie, G. M. Chow, Sol. Energ. Mat. Sol. Cel. 95 (2011) 800.
[19] D. Li, C. Ding, H. Shen, Y. Liu, Y. Zhang, M. Li, J. Phys. D: Appl. Phys. 43 (2010) 015101.
[20] J. Liu, Q. Yao, Y. Li, Appl. Phys. Lett. 88 (2006) 173119.
[21] C. J. Jia, L. D. Sun, F. Luo, X. C. Jiang, L. H. Wei, C. H. Yan, Appl. Phys. Lett. 84 (2004) 5305.
[22] D. Chen, Y. Wangn, M. Hong, Nano Energy. 1 (2012) 73.
[23] S. W. Park, H. K. Yang, J. W. Chung, Y. Chen, B. K. Moon, B. C. Choi, J. H. Jeong, J. H. Kim, Phys B. 405 (2010) 4040.
[24] U. Rambabu, D. P. Amalnerkar, B. B. Kale, S. Buddhudu, Mater. Res. Bull. 35 (2000) 929.
[25] J. E. Geusic, F. W. Ostermayer, H. M. Marcoes, L. G. Van Uitert, J. P. van der Ziel, J. Appl. Phys. 42 (1971) 1958.
[26] L. G. Van Uitert, s. Singh, H. J. Levinstein, L. F. Johnson, W. H. Grodkiewicz, J. E. Geusic, Appl. Phys. Lett. 15 (1969) 53.
[27] J. W. Stouwdam, M. Raudsepp, F. C. J. M. van Veggel, Langmuir. 21 (2005) 7003.
[28] R. Jenkins, R. L. Snyder, John Wiley & Sons, Inc. New York, p. 90 (1996).
[29] J.W. Stouwdam, F.C.M. Van Veggel, Nano Lett. 2 (2002) 733.
[30] R. Chai, H. Lian, Z. Hou, C. Zhang, C. Peng, J. Lin, J. Phys. Chem. C. 114 (2010) 610.
[31] A. Rapaport, J. Milliez, F. Szipocs, M. Bass, A. Cassanho, H. Jenssen, Appl Opt. 43 (2004) 6477.
[32] X. Qiao, X. Fan, Z. Xue, X. Xu, Q. Luo, J. Alloy. Compd. 509 (2011) 4714.
[33] K. Hara, H. Sugihara, Y. Tachibana, A. Islam, M. Yanagida, K. Sayama, H. Arakawa, G. Fujihashi, T. Horiguchi, T. Kinoshita, Langmuir. 17 (2001) 5992.